

Nonlinear dynamics and the nano-mechanical control of electrons in crystalline solids

Nano-mechanical control of electrons

M.G. Velarde^a

Instituto Pluridisciplinar, Universidad Complutense, Paseo Juan XXIII 1, 28040 Madrid, Spain

Received 28 March 2016 / Received in final form 26 July 2016
Published online 30 September 2016

Abstract. Under the umbrella of nano-mechanical control of electrons in crystalline solids, provided here are i) a discussion of aspects of the influence of static piezoelectricity on semiconductors, ii) a description of electron surfing on traveling piezopotentials/surface acoustic waves, iii) comments on the role of solitons in (dopable) polymer conductors/synthetic metals, and iv) the major component of these notes, a discussion of basic aspects of lattice solitons and discrete breathers permitting to understand genuine electron surfing on nanosolitons. This surfing offers a form of long range, fast and robust transport process in crystalline solids. The particular case of the undopable highly crystalline polydiacetylene polymer serves to illustrate the invention of a novel solectron field effect transistor (SFET).

1 Introduction

Our sensations like touch, hearing or pain follow from the conversion of mechanical stimuli into electro (chemical) signals along nerves/the neural system, from mechanoreceptors to neurons. On the other hand, the minimal act for a chemical “reaction” to occur is the transfer of an electron from one site (called it “donor”) to another (called it “acceptor”). Referring to “crystalline molecular wires” (nanowires or nanobelts; natural or synthetic DNA or other macromolecules) at the nano-level, the mechanical control of electrons offers the possibility of guiding electrons along them with velocities that could be supersonic. The latter is expected when electrons surf on lattice solitons [1]. Already using linear (albeit strong/high amplitude enough) traveling piezoelectric waves as surface acoustic waves (SAW) the electron surfing with sonic velocity has been observed though only over rather short distances on homogeneous substrates [2–19]. Appropriate (linear or nonlinear) traveling acoustic waves may help overcoming Anderson localization in (one-dimensional/1d) disordered crystal lattices thus permitting electron transport [20]. Noteworthy is the spectacular progress already achieved using the static linear piezoelectric effect in appropriate semiconductors where electrons can be mechanically guided to offer the possibility of

^a e-mail: mgvelarde@pluri.ucm.es

alternatives (nano-electric generators) to commonly used (e.g. 3V) batteries (which if small have a short finite life span), and other electronic devices like piezoelectric solar cells, light emitting diodes (LED), etc. [21–24].

In Sect. 2 the basics of piezoelectricity and its influence on semiconductors is succinctly recalled. It seems pertinent to highlight some achievements of significant technological potential in the linear world that piezoelectric-assisted mechanical control of electrons at the nanolevel has produced; then open avenues for further progress are easily seen when, in particular, we think of adding nonlinear dynamics or just nonlinear relationships among effects. Section 3 is devoted to comments on electron surfing on SAW; once more easily seen appear open lines of research. In Sect. 4 a succinct discussion is provided about the possible yet not actual role of solitons and electron surfing in conducting polymers. In Sect. 5 genuine electron surfing on solitons in anharmonic crystal lattices is presented together with a sketchy discussion about discrete breathers (*aka* intrinsic localized modes, DB/ILM) [25]. Finally, in Sect. 6 some concluding remarks are provided.

2 Static piezoelectric control of electrons and their transport in semiconductors

In 1880, the brothers P. and J. Curie discovered that in natural crystals, such as quartz, tourmaline, and Rochelle salt, “pressure” can generate electric charge. In 1881, the term “piezo-electricity” was first suggested by W. Hankel, and the inverse effect was deduced by G. Lipmann from thermodynamics principles. In the following three decades the field of piezoelectricity was established, and by 1910, W. Voigt published a standard reference monograph detailing the mechanical and electrical relationships in piezoelectric crystals. (N.B.: there are thirty-two crystal classes, twenty-one of these do not have a center of symmetry, and only twenty are piezoelectric).

Elasticity refers to the relationship between mechanical stress and strain. For small stress-strains, most elastic materials, exhibit linear behavior (Hooke’s law). Piezoelectricity is the electric polarization produced in certain materials in response to an applied mechanical stress, hence a relationship between elasticity (strain in the form of compression-stretching, bending or torsion) and electricity (exhibited in the distribution of charges on the surface of the material). To a first approximation, the electric polarization is proportional to the stress and its direction reverses if the sign of stress changes. This direct piezoelectric effect is always accompanied by the inverse piezoelectric effect which refers to the mechanical deformation (changes in shape and/or size) caused by an applied electric field/voltage drop in these materials (the direct effect is usually explored to produce sensors while the inverse effect is used for actuation purposes). Clearly, the first approximation to piezoelectricity is restricted to linear elasticity as well as linear mechanical-electrical relationship. Besides the mentioned materials, certain ceramics, polymers, biological and some other materials, insulators or semi-conductors, are piezoelectric.

Referring to static piezoelectricity the electronic and photonic communities are particularly interested on it because materials like wurtzite-structured materials (ZnO, ZnS, GaN, InN, ...) simultaneously exhibit semiconductor and photon excitation properties. Their common crystalline specificity is the lack of the earlier mentioned central symmetry which naturally produces piezoelectricity once the material is strained, thus leading to a potential drop along the straining direction in the crystal. The coinage of piezotronics (2007) and piezophotonics (2010) is attributed to Z.L. Wang [21] who wanted to emphasize that one can utilize the deformation imposed by a substrate to induce electric signals that can be used directly for controlling, e.g., Si-based electronics thus permitting direct generation of digital signals

and control using mechanical actions. In short piezotronics is for devices fabricated using the piezopotential as a “gate” voltage to control the transport of electrons or positive holes across a junction like a metal-semiconductor/M-S interface. Optoelectronics corresponds to using electronic devices to produce, harvest and control light. Electroluminescence and photovoltaics are two major effects adopted in optoelectronic devices. Being reverse processes to each other, both utilize the p-n junction or its derivatives to transfer energy between electrons, (positive) holes and photons. By further introducing piezoelectricity into play, we have piezophotonics as a three way coupling process with the piezopotential significantly enhancing the performance of optoelectronic devices. Referring to electronics of standard use the functionality offered by piezotronics and piezophotonics is a bonus to Si-based CMOS technology. In particular, due to their versatile functionality and tunable semiconducting properties, piezoelectric nanowires (NW, single or in piles) offer significant potential for applications in electronic, sensing and energy harvesting devices. Micro electro mechanical systems (MEMS) need low power, in the range of microwatts; accordingly piezoelectric approaches are among the most common and practical in MEMS scale energy harvesters. Finally, as a curiosity already operating at night clubs and railway stations, note that in our environment there is much wasted mechanical energy (dancing, walking). This ambient source of energy can be converted to useful electrical energy by piezoelectric transducers [21–24].

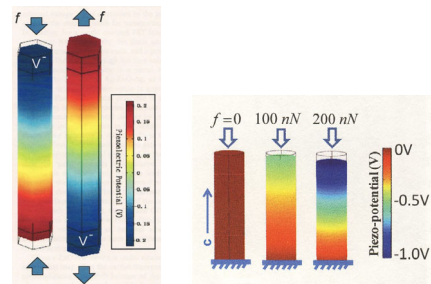


Fig. 1. Piezoelectricity and (static) piezopotential. Left block panel: typical piezoelectric response (voltage drop/piezopotential across opposite faces as shown in the right column) due to compression (left panel) and stretching (center panel) along the longest axis of a ZnO wurzite crystal of 600 nm height and 25 nm hexagonal side (compression-stretching, bending and twisting all offer chances for piezopotential). Right block panel: predicted values for a nanowire (100 nm in length and 50 nm in width) when applying a varying compression force, $f = 0, 100, 200$ nN providing about 1 V drop (adapted from figures in [21]; with permission, courtesy of Prof. Zhong Lin Wang).

To make this section a bit more complete, albeit remaining at the qualitative level, it seems pertinent to add a few more lines on how piezotronics works. At an M-S interface the Fermi level of the latter will be aligned with that of the former, leading to redistribution of charges at the junction area. Depending on the types of materials, either Ohmic contact or Schottky contact (rectifying junction) may be formed. The piezopotential modulates the interfacial energy at the junction area. The modulation can be directly reflected by the effective resistance of the junction. Accordingly, the strength of this effect is positively related to the ratio of the junction resistance to the bulk resistance. Thus the Schottky barrier is the prerequisite for the piezopotential to control electrons at the M-S interface. By applying strain to the piezoelectric semiconductor, either positive or negative polarization charges are induced at the contact interface. Taking n-type semiconductor as an example, positive polarization charges

attract free electrons and decrease the level of depletion, leading to reduced Schottky barrier height as well as its effective resistance; negative charges repel electrons and increase the level of depletion, leading to increased Schottky barrier height as well as its effective resistance. This is how the piezopotential modulates the electron transport across the M-S interface. When two semiconductors are brought into contact (n-n, p-p and p-n interfaces) their difference in Fermi levels will give rise to energy barriers at the contact interface. For the same reason, if polarization charges are introduced, the energy barrier height will be modulated accordingly.

Now let us turn to open lines of research. Four state variables are involved in the piezoelectric relations: two from elasticity/mechanics (mechanical stress and mechanical strain) and two from electricity (electrical field, and electrical displacement or otherwise polarization or static piezopotential). Experimental data show that the relations between these variables may not be linear, the high loading regime being the obvious mechanical case. When linear, the corresponding constitutive relations are derived from quadratic energy relations/Hamiltonian (which in the mechanical part originate in harmonic interactions between atoms in a crystal). A general approach to establish nonlinear constitutive relations is to consider higher order terms in the Hamiltonian or otherwise said building e. g. for mechanics upon anharmonic interactions. In some materials (like GaAs and InAs) it has been established that the piezopotential in response to crystal deformation has strong contributions from second-order terms in such a way that linear and quadratic contributions have the opposite effect on the electric field, and for large strains the quadratic terms even dominate eventually leading to a sign reversal of the piezopotential. This feature may be significant for nanostructures (like ZnO nanowires), their functions like in energy harvesting devices and their stability. It has been claimed [26] that nonlinearities in the piezoelectric field in certain materials (heterostructures like wurtzite InGaN) may lead to new areas of exploitation for optical devices such as quantum sources of entangled photons or novel LED with significantly increased efficiency relative to those commonly used today. Little has been explored along these lines of thought [26–39]. Furthermore, hysteresis and creep are also among the mechanical nonlinearities. Hysteresis means shortcoming, or delay. Creep is a time-dependent response to a constant load over an extended period of time. In piezoelectric materials, hysteretic phenomena could result in instabilities of devices, and, moreover, the time-dependent behavior may happen under electrical and mechanical loads, items whose influence is demanding serious exploration. It seems pertinent to alert about the interest of exploring in depth the expected significant role at the nano-level of strain gradients not considered here.

Also little research has been conducted to assess the role of adding an external electric field, a line of natural development for further novel and functional piezotronic devices [40]. It seems worth recalling an observation made long ago. For “normal” materials if one applies an electric field E along some crystal axis and measures the current density j along the same direction, the Ohmic relation will be obtained so long as E is sufficiently small. It was observed, however, that there appears a breakdown of linearity in the j - E characteristic for piezoelectric semiconductors such as CdS and ZnO, -when E reaches some critical value E_c [41–43]. In a first exploration Abe [44] realized that at such value of the field strength the drift velocity, $v_d = \mu E$ (μ is the mobility) is approximately equal to the sound velocity. Since the materials are piezoelectric semiconductors, there should exist a “piezopotential” acting on the carriers, say electrons, which is generated by the lattice dynamics. If such potential is of sinusoidal form then the electrons will find their places at the trough of the potential so as to make the potential energy as small as possible (see Fig. 6 below). Thus the electrons have a tendency to move through the crystal with the sound velocity, surfing on the sound waves. If the drift velocity is below the sound velocity

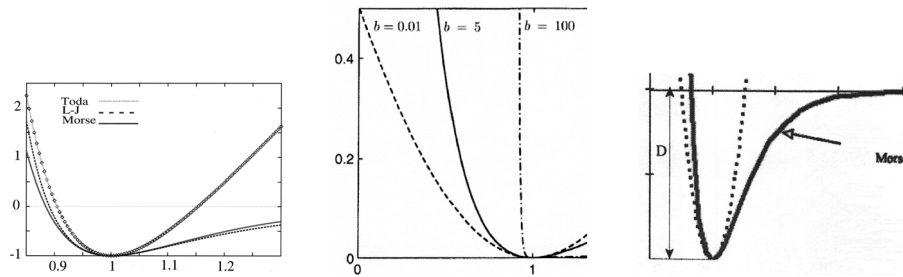


Fig. 2. Interatomic potentials (arbitrary units along the axes, just illustrating relative sizes). Left panel: Lennard-Jones, Morse and Toda interactions. Center panel: stiffness of the Morse or Toda potentials, as measured by a parameter b , from harmonic (b going to zero; $b = 0.01$) to “hard sphere” (b going to infinity; $b = 100$) interactions. Right panel: harmonic (dotted line) *versus* Morse potential illustrating, on the one hand, the lack of validity of the former when dealing with certain material characteristics like thermal dissociation, melting or thermal expansion and, on the other hand, the “softness” of the latter as the equilibrium lattice interatomic distance grows.

the electrons are accelerated by the sound waves so that energy of lattice vibration is transferred to the electrons. Then the lattice is in a damping state and nothing happens in the j - E characteristic. If, however, the drift velocity is greater than the sound velocity, electrons should give their energy to sound waves, leading to instability of lattice vibration. This instability will manifest itself as an amplification of sound waves. Actually some nonlinear mechanisms (nonlinear piezoelectricity, anharmonicity of lattice vibrations, nonlinear terms for current density) must make the (exponentially) growing amplitude saturating to a finite value; otherwise the crystal will break down. Then the electrons will pile up in the potential troughs and move with sound velocity. Consequently the current density is constant independent of E when the drift velocity exceeds the sound velocity. More on electron surfing on (surface) acoustic waves in Sect. 3, and in Sect. 4 the role of anharmonicity in the crystal lattice dynamics is considered leaving out piezoelectricity.

Finally, thinking about novel research possibilities offered by e. g. synthetic materials it seems pertinent to recall that the cubic interatomic potential is typical of crystals lacking central symmetry which is a must for piezoelectricity to exist, as already noted. Then referring to the soliton-bearing Boussinesq-Korteweg-de Vries (B-KdV) equation [45–47] it is to be noted that such potential underlies its dynamical system description. Its repulsive part does not appreciably differ from that of the Morse or the Toda potentials, the latter, like in the case of the cubic potential, not being physically acceptable in its attractive part (Fig. 1). There is more on using these potentials in Sect. 5.

3 Traveling piezopotential and the electron surfing on surface acoustic waves (SAW)

Linear and nonlinear SAW have been intensively studied since the pioneering works of Lord Rayleigh (1885) and A.E.H. Love (1911) [13–19]. A propagating SAW along a (linearly elastic) homogeneous substrate does not experience dispersion. However, most materials are not perfect and hence dispersion eventually spoils linear wave propagation beyond a rather short path. On the other hand, dispersion can be tuned according to needs if over a given material is deposited a layer of another material with appropriate thickness. If the underlying substrate is elastically nonlinear then the

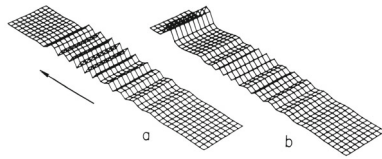


Fig. 3. Linear *versus* nonlinear waves. Schematic view of the space-time evolution, along a crystal lattice nanobelt, of a linear wave (left panel) and a nonlinear wave, eventually a solitonic wave (right panel). Starting with the same initial condition on the left (a) we see the fate of the linear wave due to dispersion whereas on the right (b) we see how nonlinearity permits piling up, hence selforganization, to a level that eventually is maintained “as long as we wish” (using the appropriate substrate, i.e., appropriate potential among the units in the lattice or otherwise appropriate heterostructures as discussed in the main text).

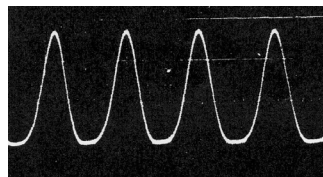


Fig. 4. SAW, cnoidal, periodic nonlinear wave typical solution of the B-KdV equation as observed by Nayanov [15] on an heterostructure formed by GaAs substrate covered by a thin film of SiO added by evaporation (courtesy of V.I. Nayanov).

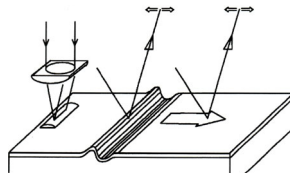


Fig. 5. SAW excitation and detection by differential interferometry. Either a beam from a single laser shining at two different spots along the path or two laser beams at a single spot permit the characterization of the SAW (adapted from a figure in [17]).

SAW produced could be a nonlinear wave eventually a solitonic wave. The latter is the kind of wave that can travel over “long distances” without altering its characteristics and with supersonic speed. Those characteristics can be modified applying electric fields or varying temperature as well as playing with the type and dimensions of the heterostructure used. Figure 3 illustrates the expected evolution of both a linear and a non-linear wave along an (ideal, quasi-one-dimensional) crystal lattice nanobelt.

Nayanov [15] used a substrate made of LiNbO_3 covered by a thin film (50 nm) of SiO deposited by evaporation. Starting with an initial sinusoidal wave he observed the evolution to a typical nonlinear wave very much like the kind of cnoidal periodic solution of the B-KdV equation [45–47]. Indeed, the combination of the substrate and the added film on top of it permitted balancing nonlinearity and dispersion. He also observed other wave forms. Hess and collaborators [16–19] used a variety of heterostructures and played with the appropriate nonlinearity of the material and the dispersion introduced by an additional film, considering both cases of normal and abnormal dispersion (long waves travel faster/slower than shorter ones, respectively). They followed the evolution of the SAW by using a set-up as schematized in Fig. 5 and observed a variety of nonlinear wave forms.

The invention of the interdigital transducer (IDT, 1965) [48], permitting conversion of electric signals in SAW and viceversa, has opened means of benefiting from

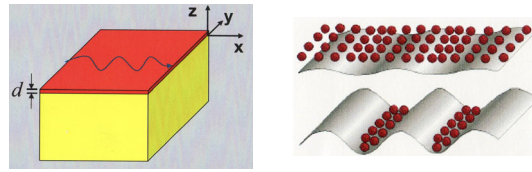


Fig. 6. SAW. Electron surfing on mechanical/surface acoustic waves. Left panel: artistic depiction of a SAW on a heterostructure with an added upper film of thickness d . Right panel: only with long lasting, strong/high amplitude enough traveling piezopotential waves electron surfing and hence electron transport is possible (adapted from a figure in the 1999 AIP free access archives).

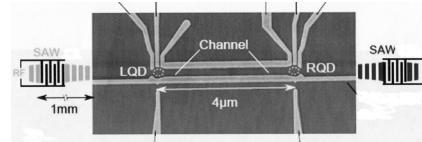


Fig. 7. SAW ping-pong table. SAW (most surely already a nonlinear wave) with surfing electrons have been observed traveling back and forth between two quantum dots (LQD, RQD) (adapted from a figure in [13]).

the controllable delay of five orders of magnitude in the propagation speed of linear acoustic waves relative to electromagnetic waves (note that a piezoelectric crystal is, in fact, an electromechanical transducer and that high voltages may bring only tiny changes in the size of the crystal). Following the pioneering work of several authors (since at least 1982) [2,3] and, in particular, A. Wixforth and colleagues [4–9] two experiments in 2011 have given “celebrity” to electron surfing in piezoelectric materials [10,11]. The experiments so far known are limited to using linear waves on perfectly homogeneous substrates. Figure 6 offers a schematic, artistic view of electron surfing on SAW, illustrating the role of wave amplitude (in the polarization field/traveling piezopotential). Wixforth and colleagues have profited from the five orders of magnitude delay in the speed of sound relative to electromagnetic waves for a variety of electronic purposes by using a double IDT (emitting-receiving) set-up, similar to the one depicted in Fig. 7, with one and the same signal splitted along two different paths, one mechanical along a material and the other traveling in free space.

The experiments of Meunier, Ford and collaborators [10–12] on GaAs substrates permitted the transfer of one or more electrons (single or pairs) from one quantum dot to another having in mind possibilities offered by SAW for quantum computation devices (thus incorporating spins). As my purpose was simply to illustrate how electrons can be mechanically controlled using traveling piezopotentials I shall not dwell here on their electronics achievements thus referring to their papers. Suffices for fun presenting Fig. 7 which illustrates the kind of ping-pong game they played with electrons going back and forth from one quantum dot to another, as earlier also done by Wixforth. This game and other achievements should be better played over quite long paths using nonlinear soliton waves of tunable speed.

4 Conducting polymers/synthetic metals and (topological) solitons

Conducting polymers belong to an affordable economically huge electronics technology that permeates our daily life. Yet everything started with the accidental, not exactly serendipitous, discovery of the “metallic” aspect of the paradigmatic, albeit

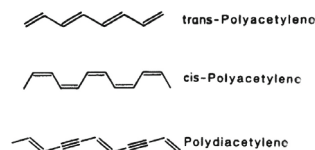


Fig. 8. tPA, cisPA and PDA illustrating dimerization (consequence of Peierls' instability for an infinitely extended crystal lattice; a gap (*ca* 1.4 eV) opens between the valence and the conduction bands and the polymer is a semiconductor). At each corner there is a CH group. Roughly a single bond contains one σ , a double bond one σ and one π , and a triple bond one σ and two π . More bonds make their total length shorter and stronger.

of not practical use, transpolyacetylene (tPA; it is easily oxidized under standard atmospheric conditions, it easily decomposes when heated instead of melting, it is easily affected by acids and electric fields tend to destroy its dimerization/conjugation) [49–59]. Since then quite many papers (well over a thousand) have been published dealing with a rich variety of conducting polymers (otherwise denoted as synthetic metals).

Figure 8 provides a schematic representation of tPA, cis-polyacetylene (cis-PA) and polydiacetylene (PDA) in their ground state. In lattice terminology the units are π -electrons (a block with single and double bonds between CH groups) whereas σ -electrons provide the stable backbone (not really affected if one π -electron goes away; though the π -electrons are weaker and more delocalized than the other they may be thought of as a practically “submerged” in a larger sea of σ -electrons). Focusing on tPA we note that the single bond is longer than the double bond, $L_1 > L_2$ (approximately $L_1 = 1.44 \text{ \AA}$, $L_2 = 1.36 \text{ \AA}$; in energy terms a single bond is *ca* 3.6 eV and a double bond *ca* 5 eV hence shorter and stronger). As the orientation of the bonds is twofold there is degeneracy of its ground state. Hence a defect is the only possible way of joining them (both configurations belong to the same energy level; Fig. 9). This defect is a kink (*aka* topological soliton of zero charge and spin 1/2 as there is an impaired π -electron; though it contains one electron it is a neutral free radical). When a π -electron is removed by e.g. doping by oxidation the defect remains and hence the soliton becomes positively charged (p-doping; it leaves a positive hole albeit with zero spin/radical cation) while reduction adds a second electron to the defect, giving it a negative charge (n-doping) but still zero spin. At variance with conventional materials this symmetry breaking of the charge-spin relationship is specific to “infinitely extended” systems with degenerate ground state. Figure 10 illustrates the movable character (translational invariance) of the soliton as well as that of a polaron, the latter being the bound state of a charged soliton and a neutral soliton; when two charges with opposite spins are trapped or lost thus leaving two positive holes the excitation becomes a bipolaron).

The basics of tPA dynamics is beautifully contained in the so-called SSH Hamiltonian whose core is a harmonic lattice backbone augmented with the evolution of an added excess charge in the tight binding approximation (TBA) [52]:

$$\mathcal{H} = \sum_{n,s} (t_{n-1,n} a_{n+1,s}^+ a_{n,s} + h.c.) + (K/2) \sum_n (u_{n+1} - u_n)^2 + (M/2) \sum_n (du_n/dt)^2 \quad (n = 1, \dots, s = \pm 1/2), \quad (1)$$

where u_n accounts for the distortion (relative to equilibrium) of the n th unit (single and double bond together) along the lattice (*ca* 0.04 \AA). There is an additional factor $u_n = (-1)^n u$ to account for the dimerization. This degeneracy of the ground state

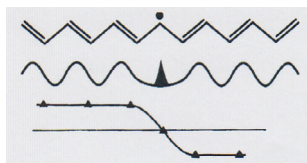


Fig. 9. tPA. Defect/kink/topological soliton: Due to the degeneracy of the ground state its two dimerized configurations (upper panel) join via a defect (dotted peak). The center panel illustrates the corresponding charge density wave peaked at the defect. The bottom panel illustrates the defect as a tanh-like topological soliton when plotting the values of the so-called “alternation” parameter $(L_1 - L_2) / [(L_1 + L_2) / 2]$ around the defect.

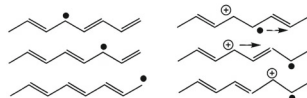


Fig. 10. Soliton and polaron in tPA. Left panels: movable/translationally invariant soliton (neutral, no charge transport). Right panels: movable positive hole polaron. Similar figures are for charged (electron or positive hole) solitons and for an electron polaron (which is the lowest energy excitation in tPA).

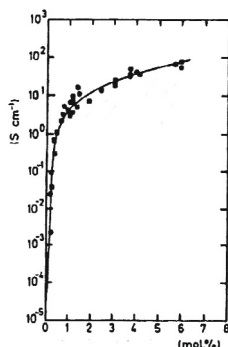


Fig. 11. tPA (dc) conductivity *versus* doping fraction (adapted from [52, 53, 60, 61]).

(Fig. 9, upper panel) is incorporated by completing (1) with a double well quartic potential. Then the soliton solution of such (nonlinear) SSH dynamics comes naturally as $\phi_n = \tanh[(n - n_0)a/\xi]$, centered at n_0 , with n going to plus and minus infinity; ξ is its reticular extension (Fig. 9, bottom panel). K (*ca* 20 eV/Å²) is the elastic (linear, Hooke) constant of the σ “springs” (in the potential energy) and M (*ca* 10⁻²³ g) is the mass of the CH unit (in the kinetic energy). The operators $a_{n,s}^+ / a_{n,s}$ create/annihilate a π -electron of spin s at the n th CH site. The factor $t_{n+1,n} = t_0 - \alpha(u_{n+1} - u_n)$, t_0 to first approximation in the TBA, estimates the energy for a nearest-neighbor hop (the matrix elements account for overlapping or hopping integrals in the kinetic energy of the π -electrons); t_0 (1–3 eV) is the value prior to dimerization and α (*ca* 4 eV/Å) estimates the electron-phonon (lattice) interaction following dimerization (before its value is zero). The quantities t_0 and α parameterize the Coulomb repulsion among π -electrons. Since $a_{n,s}^+ a_{n,s}$ annihilates an electron on site (n) and creates one on site ($n + 1$), in this way an electron moves (hops) from site (n) to site ($n + 1$). Thus the first term of (1) represents the kinetic energy of the π -electron.

Figure 11 depicts experimental data on the (dc) electric conductivity, going from about 5×10^{-5} S/cm, a practical insulator when undoped, to become a good

(synthetic) metal as the doping fraction is increased. Yet an open question still remains many years after the discovery of conducting polymers: what the actual transport mechanism is. In view of the soliton solution of the SSH dynamics (Fig. 9) the first idea was that transport could have been with charged solitons, later on the suggested carriers were polarons and even bipolarons (hence transport via bosons) [55–58]. Noticeable is that, at variance with metals, the conductivity of tPA (and others) increases with increasing temperature, a fact that still is in demand of a satisfactory explanation. In view of the messy structure of tPA as a bunch of interlaced “fibrils” (like spaghetti), as shown with high resolution electron microscopy, another idea was that transport was saltative from one fibril to another and so on, and hence essentially three-dimensional; even the fibrils were supposed to be formed of fine metallic balls linked together [56]. For light to moderately doped samples Mott’s variable range hopping [62–64] seems to work but no one mechanism seems to apply to tPA over the whole range of doping. I come back to the SSH Hamiltonian and to the concept of genuine soliton-assisted charge transport in the next section.

5 Lattice solitons and discrete breathers (DB/ILM). Electron surfing on anharmonic crystal lattices

5.1 Nanoscale lattice solitons and discrete breathers

The study I wish to refer now, albeit in succinct presentation, is based on a “natural” extension -still in 1d- of the SSH Hamiltonian, obtained by replacing the harmonic backbone lattice intersite potential with the Morse potential or some other similar anharmonic one:

$$H_{lattice} = \sum_n [(p^2/2M) + V(r)], \quad (2)$$

where, as in (1), referring to lattice units/“atoms”/sites, p , M and r denote, respectively, momentum, mass of unit “n” and interatomic distance. For Morse interactions we take:

$$V(r) = (a/2b) (e^{-2br} - 2e^{-br}) = D (e^{-2br} - 2e^{-br}), \quad (3)$$

where D is the potential depth (or dissociation energy; $D = a/2b$, with a and b denoting, respectively, the linear Hooke elastic constant and the (anharmonic) stiffness of the intersite “springs”) (Fig. 2). The lowest order hence harmonic vibration is $\omega_M = (ab/M)^{1/2} = (2Db^2/M)^{1/2}$. Referring to relative intersite motions we set $q_n = b(u_n - \sigma)$, with σ , here the equilibrium value (*ca* 1–3 Å). The q_n may not be limited to infinitesimal elongations and could go beyond, say, 0.04 Å. To be recalled is that in 1d the kinetic energy is twice the potential energy.

The dynamical system (2)–(3) is integrable for the Toda interaction (Fig. 2). For the non integrable case with Morse interaction the solution has been obtained numerically and the results are within ten percent error relative to the exact Toda solutions found analytically [45]. Note that solitons are predicted in the sloped region of the specific heat (at constant length), *versus* temperature, past the Dulong-Petit plateau (Fig. 12, right panel). This result is confirmed by the computation of the dynamic structure factor (frequency spectrum of the correlations between density fluctuations for a given wave vector in the crystal) (Fig. 13), a typical quantity for experiments with thermal neutron scattering.

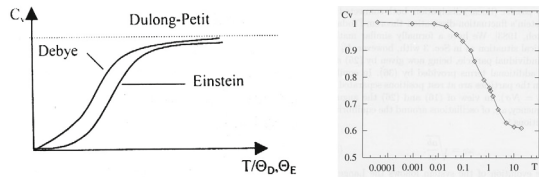


Fig. 12. Specific heat at constant volume/length. Left panel: predictions of Einstein and Debye theories (the latter agreeing with experiment at low temperatures) ending in the classical Dulong-Petit plateau at high enough temperatures (curves rescaled with their corresponding Debye and Einstein temperatures). The right panel illustrates, for a Morse lattice, the Dulong-Petit plateau and its continuation as the temperature increases on the way to melting. It is along the sloped region (0.1–1) where solitons are predicted for a Morse (and also a Toda) lattice agreeing with the prediction of the dynamical structure factor as depicted in Fig. 13. Along the abscissa T is rescaled with the well depth of the potential (see main text).

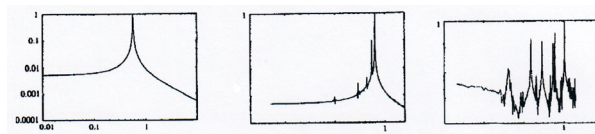


Fig. 13. Morse lattice. Dynamic structure factor (suitably rescaled for illustrative purposes) versus frequency as a function of increasing temperature below (left panel) at (center panel) and above (right panel) the expected transition, along the sloped region in Fig. 12. We can observe the transition from phonons to a messy background where the soliton emerges in a Toda or Morse lattice (highest peak at extreme right). The value “1” along the abscissa indicates the dimensionless sound velocity and hence the soliton appears with supersonic speed (adapted from figures in [66]).

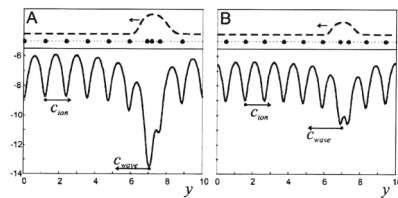


Fig. 14. Morse lattice (2)–(3). The upper portion in the left panel corresponds to three atoms compressed to being quite near to each other whereas in the right panel the corresponding compression is weaker and affects only a couple of atoms. The middle rows show the atoms along the lattice. The lower portions of the panels depict the corresponding traveling polarization field. Further details are given in the main text (compare to SAW piezopotential in Figs. 4 and 6).

Although further below the complete classical-quantum dynamics of the problem is explicitly provided it seems pertinent before doing this to introduce just a phenomenological first approach, built upon the classical Drude-Lorentz theory, in order to compare with what was earlier presented about SAW (though no piezoelectricity is invoked in this section) [65,66]. For an added excess electron to the ions in the lattice, Fig. 14 qualitatively shows the electric polarization field consequence of a local compression along the horizontal axis y . In the reference frame of the atoms, the lattice deformation appears as a soliton correlated to a polarization wave which is

very much like the SAW earlier described (Fig. 6). There is a difference; here there is a “single” deepest well/trough whose depth depends on the actual finite amplitude local lattice compression (stronger in the left panel relative to the right panel). Otherwise all the troughs would have the same depth and would be placed one at each atom site. If atoms were considered moving (c_{ion} to the right) then the solitonic wave moves (c_{wave}) in the opposite direction to that of the overall atomic motions. Such a behavior is quite the same as that of the solitonic bore wave (hydraulic jump) in a river which travels upstream while the water flows downstream towards, say, the sea (recall Figs. 9 and 10). Here the added, excess electron would fall in the deepest trough and, only in it, would be moving bound to it as a surfing motion. In the SAW case electrons are transported/surf trapped using each and every single trough of the traveling piezopotential.

As noted above, the interaction considered in the Hamiltonian (2)–(3) refers to change in relative intersite distances and hence longitudinal motions. Noteworthy is that the particular Morse potential (3) is a “soft” potential in the sense that when widening the intersite/atomic separation it is of weaker strength than the linear Hooke/harmonic spring. Or otherwise said the frequency of small amplitude oscillations around the minimum decreases with increasing amplitude. The converse case is considered as a “hard” potential. It turns out that discreteness in a lattice provides bounds and gaps to the spectrum of linear oscillations whereas nonlinearity makes the amplitude of oscillation frequency-dependent. The combination of discreteness and nonlinearity has led to the finding of a form of local excitation denoted intrinsic localized mode (ILM) or otherwise said discrete breather (DB) [25, 67–79], a surprising finding as the lattice might be quite perfect defect less. DB could be mobile, subsonic or otherwise, pinned or even impossible depending on parameter values in the potentials. Inside the phonon band DB/ILM are not possible since any resonance of their harmonics with the extended phonons will radiate the DB/ILM away. They can only appear below or above the phonon band. Accordingly, they cannot decay by emitting linear radiation/phonons. (N.B.: Following [74], “a DB is a localized, oscillatory excitation that is stabilized against decay by the discrete nature of the periodic lattice”; “an ILM is an excitation that is localized in space by the intrinsic nonlinearity of the medium, rather than by a defect or impurity”; a more comprehensive mathematical description is given by Iooss and James [75]). This is at variance with common lattice solitons, corresponding to atomic lattice longitudinal elongations, which are generally supersonic moving localized excitations like those exhibited by the Toda or Morse lattices [45–47]. If to longitudinal elongations we add onsite vibrations and, accordingly, we add an onsite potential at each lattice site then the picture becomes rich of possibilities. For instance localized modes could be pinned or mobile depending not only on parameter values in the absolute sense but also on the ratio of the stiffness and depth of the intersite and onsite potentials involved in the dynamics. DB/ILM are to be expected when strong onsite potentials compete with weak intersite interactions as the latter may allow one kind of “opportunistic”/selfish or cooperative atom (think about spontaneous fluctuations) to start profiting from the support of the neighboring others to grow above the rest.

In view of the above a series of numerical experiments have been conducted with a lattice whose dynamics is governed by intersite elongations obeying Morse potentials and onsite vibrations also obeying Morse potentials, albeit with controllable ratios of spring stiffnesses and potential well depths. Figure 15 illustrates the supersonic traveling soliton found when the onsite potentials are switched off, whereas Fig. 16 illustrates the extreme opposite case when the intersite potentials are practically switched off and a pinned DB/ILM appears. The space-time evolution of localized excitations between these two extreme cases has been provided in Ref. [80].

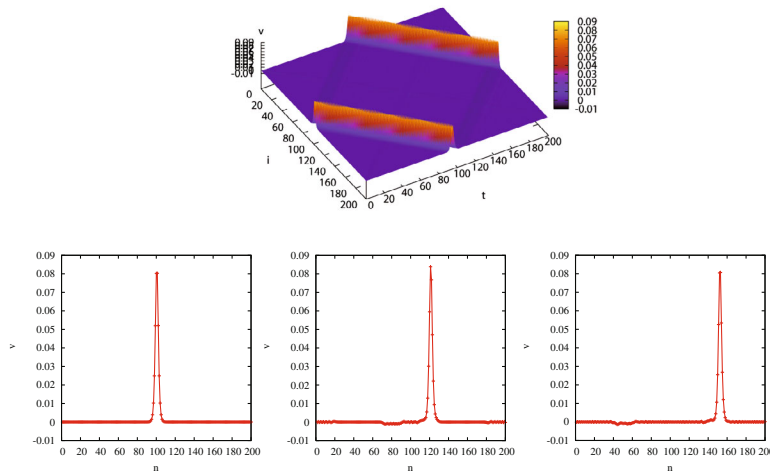


Fig. 15. Typical lattice soliton in a 1d lattice with only intersite Morse interactions (and periodic boundary conditions). The upper panel shows the actual motion along a lattice of two hundred units during two hundred time units (made dimensionless using as scale the inverse of the harmonic vibrations around the minimum of the potential well). Lower panels illustrate, from left to right, the velocity as a defining quantity at time instants $t = 10, 20$ and 50 , in appropriate dimensionless units (see main text). Motion is supersonic with value 1.05 the sound velocity (adapted from figures in [80]).

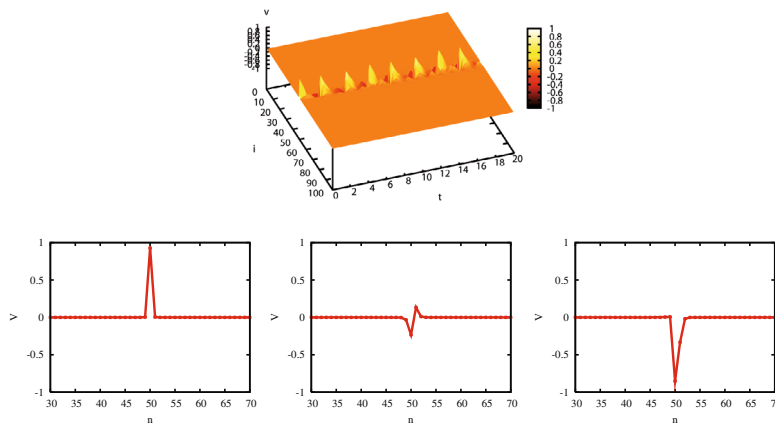


Fig. 16. Typical DB/ILM in a 1d lattice with strongly dominating onsite Morse interactions (and periodic boundary conditions). The upper panel shows the actual motionless character of the local excitation. The lower panels show how there is local periodic alternance between a maximum and a minimum as time proceeds, for time instants $t = 0.1, 1.2$ and 2 in appropriate dimensionless units (see main text) (adapted from figures in [80]).

5.2 Electron surfing on nanoscale lattice solitons

Focusing on lattice solitons with (2)–(3), then for the electron again the TBA is used, see Eq. (1). In terms of probability density coefficients we have:

$$H_e = \sum_n E_n(q_n) c_n c_n^* - \sum_n V_{n,n-1}(q_n) (c_n c_{n-1}^* + c_n^* c_{n-1}), \quad (4)$$

with

$$E_n = E_n^0 + \chi_0 q_n + \chi_1 (q_{n+1} - q_{n-1}) + \dots \quad \text{and} \quad V_{n,n-1} = V_0 \exp[-\alpha (q_n - q_{n-1})], \quad (5)$$

where following Slater the matrix elements (overlapping or hopping integrals between nearest-neighbors) are taken in exponential form [81, 82]. Clearly, Taylor expanding (3) and (5) and inserting the first approximation in (2) and (4) we get the core SSH Hamiltonian (1). The parameter α regulates how much the $V_{n,m}$ ($E_{n,m}$ in (1)) are influenced by the corresponding intersite separations, $(q_n - q_{n-1})$. In the simplest case it is enough to account for the compound product αV_0 (earlier αt_0 in (1)). The case $\alpha = 0$ was considered by Davydov and numerous other authors to discuss models for charge transfer in proteins and other biomolecules albeit with not much realistic success [83–85].

To make the description of universal value all quantities can be rescaled (marked with tilde) using new units. Thus we set $V = V_0/2D$, $\tilde{\alpha} = \alpha/b$, $\tau = V_0/h\omega_M \sim 10-20$ and $\epsilon_n^0 = E_n^0/h\omega_M$. Accordingly, in terms of energy we have:

$$E_n = [\epsilon_n^0 + \tilde{\chi}_0 \tilde{q}_n + \tilde{\chi}_1 (\tilde{q}_{n+1} - \tilde{q}_{n-1})] |c_n|^2 - 2\tau \sum_n \text{Re}(c_{n+1} c_n^*) \exp[\tilde{\alpha} (\tilde{q}_n - \tilde{q}_{n+1})]. \quad (6)$$

In what follows we delete the tilde, for simplicity. Then from the complete Hamiltonian (2)–(4) the following equations of motion are obtained:

$$\begin{aligned} d^2 q_n / dt^2 = & [1 - \exp(q_n - q_{n+1})] \exp(q_n - q_{n+1}) \\ & - [1 - \exp(q_{n-1} - q_n)] \exp(q_{n-1} - q_n) \\ & + 2\alpha V \{ \text{Re}(c_{n+1}^* c_n) \exp[\alpha (q_n - q_{n+1})] - \text{Re}(c_n c_{n-1}^*) \exp[\alpha (q_{n-1} - q_n)] \} \\ & + (V/\tau) [-\chi_0 |c_n|^2 + \chi_1 (|c_{n+1}|^2 - |c_{n-1}|^2)], \end{aligned} \quad (7)$$

$$\begin{aligned} i (dc_n / dt) = & [\epsilon_n^0 + \chi_0 q_n + \chi_1 (q_{n+1} - q_{n-1})] - \\ & \tau \{ c_{n+1} \exp[\alpha (q_n - q_{n+1})] + c_{n-1} \exp[\alpha (q_{n-1} - q_n)] \} \\ & - (n - n_{el}) E c_n. \end{aligned} \quad (8)$$

The latter is the lattice discretized Schrödinger equation. For completeness we have added an external electric field, with E and \hat{E} such that $E = (h\omega_M/\sigma e)\hat{E}(V/m)$ (no confusion expected with former use of the same symbol to denote energy). It seems clear that the the external electric field is capable of altering the lattice dynamics and hence affecting acoustic excitations (waves, phonons, solitons) in the system.

The Eqs. (7) and (8) are a mixed classical-quantum system that is to be integrated using periodic boundary conditions, $q_{N+1} = q_1$ and $dq_{N+1}/dt = dq_1/dt$, and initial conditions, recalling the conservative character of the dynamics and the probability density constraint for the electron $\sum_n |c_n|^2 = 1$. To a first approximation we can restrict to $\chi_0 = \chi_1 = 0$ and ϵ_n^0 can be eliminated by rescaling the reference energy level. Quite many results have been obtained for such a dynamical system (and its extensions to 2d geometries) [65, 66, 86–91]. Suffices now to say that following a short transient quickly the electron of (8) (in probability density) is trapped by the soliton wave of (7) thus forming a bound state which has been denoted a solectron. The latter is the natural generalization of the commonly used polaron concept (and charge carrier). It is just another form of expressing the electron surfing on the mechanical, acoustic lattice soliton wave, very much as in the above mentioned cases of

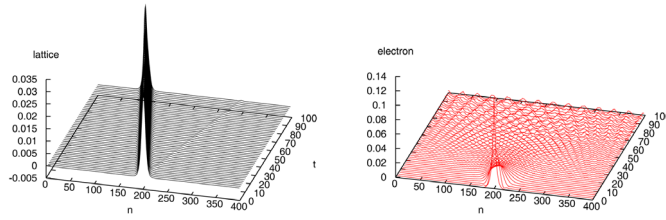


Fig. 17. Separate evolution of soliton in a Morse lattice (left panel) and of an electron (right panel) as provided by Eqs. (7) and (8) when $\alpha = V = 0$. Initially both are localized at site 200. The soliton evolves almost unaltered whereas the electron peaked at the initial time “uniformly” spreads all over the lattice in accordance with Schrödinger equation (adapted from figures in [86]).

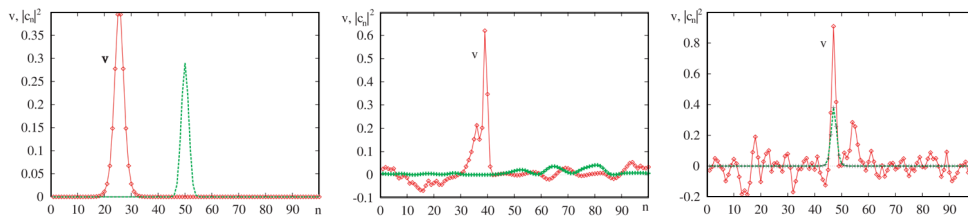


Fig. 18. Morse lattice. Alternative view of the process described in Fig. 17 (extreme left and center panels) accompanied by the predicted evolution (extreme right panel) of the soliton (initially placed at site 25) and the electron (initially placed at site 50) first when $\alpha = V = 0$ and subsequently (extreme right panel) when α and V are non vanishing. It appears that the soliton gathers the tiny (practically) uniform electron probability density piling it up to a peak around itself (kind of vacuum cleaner process) and then travels as a solectron bound state.

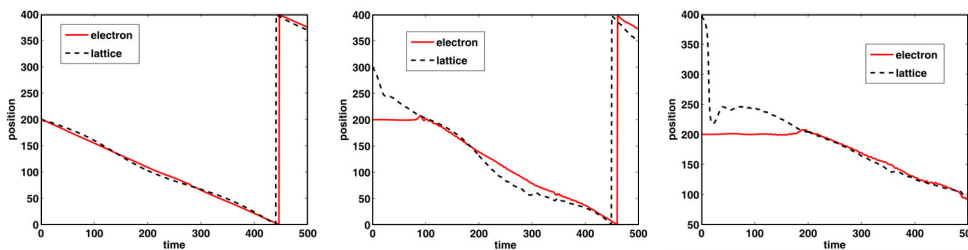


Fig. 19. Morse lattice. Space-time trajectories of the soliton and the electron when the former is placed at sites 200, 300 and 400 whereas the latter is always localized at site 200 at the initial time. Following a short transient the soliton manages to catch the electron (in probability density) thus forming the solectron bound state. Needless to say there is also a polaron process which we do not consider here for simplicity (adapted from figures in [86]).

electron surfing on traveling piezopotential waves and SAW. To be noted is that the soliton exists alien to the presence of an excess electron which is at variance with the polaron concept where it is the electron that selftraps thus creating the new charge carrier. In the present case there is indeed the action of the two influences, polaronic and solitonic [88]. Figure 17 illustrates how a soliton and an electron evolve separately. Figures 18 and 19 depict how a lattice soliton and an (excess) electron evolve in space and time either separately (Fig. 18, extreme left and center panels) or bound

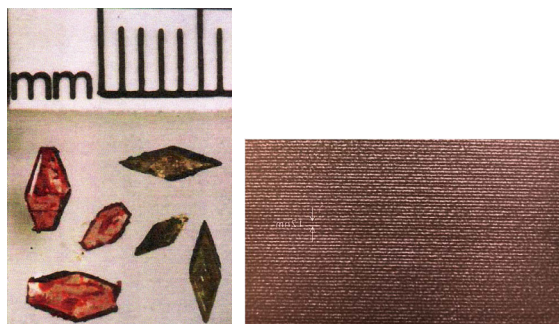


Fig. 20. PDA. Left panel: perfect crystals of mm size. Right panel: PDADCH high resolution electron microscope picture with 1.2 nm separation between lines (courtesy of E.G. Wilson).

together forming a sollectron (extreme right panel). Indeed if the Schrödinger equation is integrated separately alone ($\alpha = V = 0$), the electron as time proceeds “diffusively” becomes delocalized all over the lattice ring (Fig. 18, center panel). Then when, after the delocalization is established, α and V are switched-on, hence nonvanishing, soon the electron becomes trapped by the lattice soliton as the latter forces reconstruction of a peaked electron probability density around itself in a kind of “vacuum cleaner” process (Fig. 18 extreme right panel).

5.3 Electron surfing on nanoscale lattice solitons in PDA and related crystalline polymers and the sollectron field effect transistor

In 1987 PDA was included in the list of most important conjugated polymers. It was unique in offering magnificent crystals of mm size (Fig. 20, left panel). Added to PDA are its sulfonate derivatives PDATS [$(=CR-CtC-CR=)_n$, t: triple bond, R: $-CH_2-O-SO_2-C_6H_4-CH_3$] or PDADCH (the lateral group DCH contains di-N-carbazolyl). As the right panel of Fig. 20 shows, PDADCH is indeed a polymer comprised of π -conjugated carbon chains, perfectly parallel, and separated from each other by a distance large compared to electron wave function overlap (π -electron transfer between chains is not possible). Thus, each chain is an ideal one dimensional electronic system. In the fashion of three decades ago the overwhelming majority (almost hundred per cent scientists working in the field) disregarded the highly crystalline polymer PDA and the work done on it as, at variance with what tPA and similar dopable polymers offered, no particularly interesting electric conduction was measured being non dopable [52]. It is a remarkable fact that sollectron propagation was experimentally stumbled upon [92–96]. Donovan and Wilson found a charge carrier which moved at a velocity of close to the sound velocity, unchanged when the electric field was varied by four orders of magnitude (recall the above mentioned behavior of piezoelectric semiconductors like CdS and ZnO [41–44]; PDA is not piezoelectric). The velocity was measured for fields from 10^2 to 10^6 volts per meter, and was constant. The sollectron travelled almost mm distance before trapping, transiently, at some defect thus reflecting the purity and perfection of the polymer chains.

In order to refer to the mentioned experiments by Donovan and Wilson [92–95], for illustration one chain is modeled by a lattice with four hundred units. To simplify, the internal structure with single, double and triple bonds of the lattice unit is neglected [91]. Then using Eqs. (7)–(8) with periodic boundary conditions, to simplify their integration, as initial condition ($t = 0$) is taken the soliton of the Toda

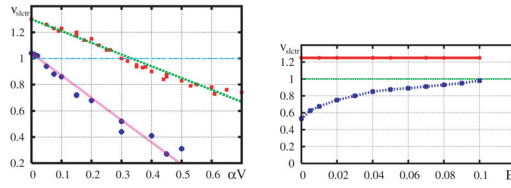


Fig. 21. PDA. Left panel: sollectron velocity, v_{slc} , *versus* electron-lattice interaction parameter αV , for $\kappa = 0.5$ with initial $v_{soliton} = 1.04$ (pink/bottom line) and for $\kappa = 1.35$ with initial $v_{soliton} = 1.3$ (green/upper line). Dots are computer results and straight lines approximate fits for illustration, $v_{slc} = 1.3 - 0.9\alpha V$ (upper line) and $v_{slc} = 1.04 - 1.7\alpha V$ (lower lines). Right panel: dimensionless subsonic (blue/lower curve) and supersonic (red/upper line) sollectron velocity *versus* dimensionless field strength. These are two extreme cases and life may exist in between them. The green/horizontal line at the value unity corresponds to the (linear) sound velocity. For illustration, dimensionless $E = 0.1$ corresponds to a $E = 10^6$ V/m (adapted from figures in [91]).

lattice $\exp[3(q_n q_{n+1})] = 1 + \beta^2 / \cosh^2(\kappa n \beta t)$, with the corresponding formula for its velocity; $\beta = \sinh(\kappa)$ and κ is the mid-height inverse width of the soliton (in units $1/\sigma$). At $t = 0$ the electron probability density (normalized to unity, $\sum_n |c_n|^2 = 1$) is taken as a Gaussian distribution, centered at site n_{el} , with a width σ_{el} , which is approximately that of the chosen soliton initial condition; in practical terms $\sigma_{el} = 3$ and $\tau = 10$ in all the computations. There is also the earlier assumed limitation $\chi_0 = \chi_1 = \epsilon_n^0 = 0$. Other values used are $M \sim 10^{-22}$ g, $D \sim 0.03$ – 0.3 eV, $b \sim 2$ – 5 \AA^{-1} , $\omega_M \sim 5.10^{12} \text{ s}^{-1}$ and $\omega_e \sim 10^{14} \text{ s}^{-1}$. For illustration purpose the compound αV in (7) will be used as a monitored variable parameter. Also for simplicity, the soliton and the electron are placed at lattice site 100 to rule out boundary effects. Appropriate photoexcitation is a way of doing it simultaneously for both, soliton and electron. This is not a limitation since, as earlier illustrated, wherever the electron is placed along the lattice, the soliton placed in the same or different site is always able to trap it (Fig. 19).

After a short transient, there is the formation of a bound state of the soliton with the electron which is the sollectron. The sollectron velocity (in units of sound velocity) is estimated as the slope of its trajectory in the space-time (n, t) plot. The results found are displayed in Fig. 21 [91]. Its left panel depicts the sollectron velocity v_s *versus* the compound parameter αV accounting for the electron-lattice interaction. As expected, the latter affects the soliton. Its right panel shows a domain up to, say, $E = 0.1$ where the drift velocity is field independent for quite a wide range of values of the field strength. On the other hand, in the subsonic case the drift velocity grows with the increasing field value reaching saturation at the sound velocity. That panel also shows two significant consequences. On the one hand, as the field strength goes down, an ultrahigh mobility is expected, in agreement with the experimental results (between 200.000 and 500.000 cm^2/Vs) found by Donovan and Wilson [92–96]. On the other hand, the electric field appears as a (left-right) symmetry-breaking agent. Indeed, in general, as motion is always expected even in the absence of an external electric field, once the soliton is excited, as solitons, and hence the sollectrons, can move to the left or to the right, on the average no net conduction would be the outcome. Switching on the field breaks the symmetry thus allowing one or the other to be realized. Further details can be found in Ref. [91].

Clearly the lattice soliton described in this section is different from the soliton of the SSH theory [52] which originates in the degeneracy of the ground state of their Hamiltonian for tPA. Yet, as earlier noted, once completed the SSH dynamics with the double well quartic potential the solution is a genuine (lattice) soliton. Finally,

note that the soliton-assisted (solelectron) transport theory offers universality. Indeed, besides the application here described to PDA, it can be used for other materials whose stiffness and crystal vibrations permit strong enough compressions capable of exhibiting nonlinear soliton excitations. It is one more case of mechanical control of electrons at the nano-scale [89].

As a by-product of the theory just sketched there has been the invention of a solelectron field effect transistor using PDATS and PDA (SFET; UK patent application submitted Dec. 9, 2014; Ref. GB 1421866.3 by M.G. Velarde and E.G. Wilson, coinventors). In such a field effect transistor the charge carrier in the source-drain channel is an electron solelectron and similarly a (positive) hole solelectron. The inverter is constructed from these field effect transistors and is predicted to operate at very low supply voltages. So also can circuits that rely on the inverter such as the Boolean logic gates used in computers. The gate channel insulator thickness can be large, in comparison to the silicon field effect transistor (SiFET). For in the latter the insulator thickness is constrained to be increasingly small as both the supply voltage and hence the threshold voltage, are reduced. A larger insulator thickness is desirable as it leads to a smaller gate input capacity, and so less energy consumption on switching. It can operate at quite small currents, leading to rather low quiescent energy consumption. As the inverter is constructed from two SFET the energy cost of an inverter switch scales proportionally to the square of the supply voltage, and inversely proportional to the gate insulator thickness. Thus, in view of the above much lower energy consumption is predicted using SFET compared to current silicon technology. It is necessary that the source-drain distance be sufficiently small, and the PDATS sufficiently pure, that solelectrons travel from source to drain without trapping at impurities or defects. The limit to the response time of the SFET is the transit time from source to drain.

6 Concluding remarks

Along these notes I have tried to illustrate how charge (electron or positive hole) transfer/transport can be controlled and directionally guided by “mechanical means” in e.g. semiconductor crystals either by an induced static piezopotential at a metal-semiconductor interface or by charge surfing on acoustic waves (in particular SAW). Comments have also been provided about the possible yet not actual role played by (defects/topological) solitons in charge transport in dopable conjugated conducting polymers like tPA. Special attention has been paid to the possible and eventually actual role of nonlinearity in all cases and in that of lattice solitons in anharmonic crystal lattices. In the latter case the concept of solelectron has been recalled. It is a generalization of the commonly used (Landau-Pekar) polaron concept in standard solid state physics (based on harmonic atom interactions and phonons) [1, 88, 97–99]. There is also a natural extension of the bipolaron concept which is the bisolelectron offering a bosonic way of transport [100, 101]. Noticeable is the more than “formal” equivalence between the solelectron in PDA and the polaron in tPA. The role of the solelectron quasiparticle has been shown for charge transport in the undopable PDA polymer and derivatives for which electron surfing on solitons permits a form of field independent transport. The solelectron theory has permitted the understanding of the experimental observations carried out in the 1980–90 decade by Donovan and Wilson [92–96] on PDA and derivatives though never adequately appreciated until 2014 [91]. The solelectron approach offers a novel line for progress in (anharmonic) solid state physics. As a by-product of the theory a novel field effect transistor based on the solelectron has been invented. The claims of the invention are few and straightforward with universality and not just limited to PDA and derivatives. Computation currently consumes orders of magnitude more energy in digital switching events than is

theoretically necessary according to statistical physics [102,103]; but the technology to reduce the consumption does not exist. The SFET offers a radically new idea to produce computer elements that enable switching with orders a magnitude reduction in energy consumption. Its production will lead the way to substantial energy reductions by IT industries in use of digital computers, server farms, and smart phones.

The author wishes to express his gratitude to W. Ebeling and A.P. Chetverikov for a decade of research cooperation, and to L. Bryzhik, L. Cisneros-Ake, L. Cruzeiro, S. Dmitriev, D. Hennig, V.P. Lakhno, J.-P. Launay, G. Röpke, R.G. Rubio and E.G. Wilson for many fruitful discussion meetings held at IP-UCM. E.G. Wilson has been instrumental for our understanding of the characteristics and electronic behavior of PDA and related polymers. Furthermore, without his cooperation the invention of the SFET would have not been possible.

References

1. M.G. Velarde, J. Computat. App. Math. **233**, 1432 (2010)
2. M.J. Hoskins, H. Morko, B.J. Hunsinger, Appl. Phys. Lett. **41**, 332 (1982)
3. W.J. Tanski, S.W. Merritt, R.N. Sacks, D.E. Cullen, E.J. Branciforte, R.D. Carroll, T.C. Eschrich, Appl. Phys. Lett. **52**, 18 (1988)
4. A.O. Govorov, A.V. Kalameitsev, M. Rotter, A. Wixforth, J.P. Kotthaus, K.-H. Hoffmann, N. Botkin, Phys. Rev. B **62**, 2659 (2000)
5. A. Wixforth, J.P. Kotthaus, G. Weimann, Phys. Rev. Lett. **56**, 2104 (1986)
6. M. Rotter, A.V. Kalameitsev, A.O. Govorov, W. Ruile, A. Wixforth, Phys. Rev. Lett. **82**, 2171 (1999)
7. M. Streibl, A. Wixforth, J.P. Kotthaus, A.O. Govorov, C. Kadow, A.C. Gossard, Appl. Phys. Lett. **75**, 4139 (1999)
8. S. Völk, F.J.R. Schülein, F. Knall, D. Reuter, A.D. Wieck, T.A. Truong, H. Kim, P.M. Petroff, A. Wixforth, H.J. Krenner, Nano Lett. **10**, 3399 (2010)
9. F.J.R. Schülein, K. Müller, M. Bichler, G. Koblmüller, J.J. Finley, A. Wixforth, H.J. Krenner, Phys. Rev B **88**, 085307 (2013)
10. S. Hermelin, S. Takada, M. Yamamoto, S. Tarucha, A.D. Wieck, L. Saminadayar, C. Bäuerle, T. Meunier, Nature **477**, 435 (2011)
11. R.P.G. McNeil, M. Kataoka, C.J.B. Ford, C.H.W. Barnes, D. Anderson, G.A.C. Jones, I. Farrer, D.A. Ritchie, Nature **477**, 439 (2011)
12. B. Bertrand, S. Hermelin, P.A. Mortemousque, S. Tanaka, M. Yamamoto, S. Tarucha, A. Ludwig, A.D. Wieck, C. Bäuerle, T. Meunier [[arXiv:1601.02485](https://arxiv.org/abs/1601.02485)] [[cond-mat.mes-hall](https://arxiv.org/abs/1601.02485)]
13. A. Oliner (ed.), *Acoustic Surface Waves* (Springer, Berlin, 1978)
14. A.P. Mayer, Phys. Reports **256**, 237 (1995)
15. V.I. Nayanov, JETP Lett. **44**, 314 (1986)
16. P. Hess, Phys. Today **55**, 42 (2002)
17. A.M. Lomonosov, P. Hess, A.P. Mayer, Phys. Rev. Lett. **88**, 076104 (2002)
18. A. Kolomenskii, V.A. Lioubimov, S.N. Jerebtsov, H.A. Schuessler, Rev. Sci. Instr. **74**, 448 (2003)
19. C. Eckl, A.S. Kovalev, A.P. Mayer, A.M. Lomonosov, P. Hess, Phys. Rev. E **70**, 046604 (2004)
20. A. Ranciaro Neto, M.O. Sales, F.A.B.F. de Moura, Solid State Commun. **229**, 22 (2016)
21. Z.L. Wang, *Piezotronics and Piezo-Phototronics* (Springer, Berlin, 2012)
22. Y. Hu, Z.L. Wang, Nano Energy **14**, 3 (2015)
23. Y. Liu, Y. Zhang, Q. Yang, S. Niu, Z.L. Wang, Nano Energy **14**, 257 (2015)
24. X. Wen, W. Wu, C. Pan, Y. Hu, Q. Yang, Z.L. Wang, Nano Energy **14**, 276 (2015)
25. S.V. Dmitriev, E.A. Korzinova, Yu.A. Baimova, M.G. Velarde, Phys. Uspekhi **59**, 446 (2016)

26. M.A. Migliorato, J. Pal, R. Garg, G. Tse, H.Y.S. Al-Zahrani, U. Monteverde, S. Tomic, C.-K. Li, Y.-R. Wu, B.G. Crutchley, I.P. Marko, S.J. Sweeney, *AIP Conf. Procs.* **1590**, 32 (2014)
27. R. Gausmann, W. Seemann, *PAMM Proc. Appl. Math. Mech.* **2**, 64 (2003)
28. G. Bester, X. Wu, D. Vanderbilt, A. Zunger, *Phys. Rev. Lett.* **96**, 187602 (2006)
29. G. Bester, A. Zunger, X. Wu, D. Vanderbilt, *Phys. Rev. B* **74**, 081305 (2006)
30. R. Tao, G. Ardila, L. Montes, M. Mouis, *Nano Energy* **14**, 62 (2015)
31. S.C. Stanton, A. Erturk, B.P. Mann, D.J. Inman, *J. Appl. Phys.* **108**, 074903 (2010)
32. S.C. Stanton, C.C. McGehee, B.P. Mann, *Physica D* **239**, 640 (2010)
33. M.A. Migliorato, D. Powell, A.G. Cullis, T. Hammerschmidt, G.P. Srivastava, *Phys. Rev. B* **74**, 245332 (2006)
34. R. Garg, A. Hüe, V. Haxha, T. Hammerschmidt, G.P. Srivastava, *Appl. Phys. Lett.* **95**, 041912 (2009)
35. J. Pal, G. Tse, V. Haxha, *Phys. Rev. B* **84**, 085211 (2011)
36. H.Y.S. Al-Zahrani, J. Pal, M.A. Migliorato, *Nano Energy* **2**, 1214 (2013)
37. J. Pal, M.A. Migliorato, C.-K. Li, Y.-R. Wu, B.G. Crutchley, I.P. Marko, S.J. Sweeney, *J. Appl. Phys.* **114**, 073104 (2013)
38. G. Tse, J. Pal, U. Monteverde, R. Gang, V. Haxha, M.A. Migliorato, S. Tomic, *J. Appl. Phys.* **114**, 073515 (2013)
39. Y. Fan, X. Ji, X. Liu, P. Cai, *Wave Motion* **51**, 798 (2014)
40. F. Xue, L. Zhang, X. Feng, G. Hu, F.R. Fan, X. Wen, L. Zheng, Z.L. Wang, *Nano Res.* **8**, 2390 (2015)
41. A.R. Hutson, J.H. McFee, D.L. White, *Phys. Rev. Lett.* **7**, 237 (1961)
42. R.W. Smith, *Phys. Rev. Lett.* **9**, 87 (1962)
43. J.H. McFee, *J. Appl. Phys.* **34**, 1548 (1963)
44. R. Abe, *Prog. Theor. Phys.* **31**, 957 (1964)
45. M. Toda, *Theory of Nonlinear Lattices*, 2nd. edn. (Springer, Berlin, 1989)
46. V.I. Nekorkin, M.G. Velarde, *Synergetic Phenomena in Active Lattices. Patterns, Waves, Solitons, Chaos* (Springer, Berlin, 2002)
47. T. Dauxois, M. Peyrard, *Physics of solitons* (Cambridge University Press, Cambridge, 2006)
48. R.M. White, F.W. Volmer, *Appl. Phys. Lett.* **7**, 314 (1965)
49. H. Shirakawa, in I. Grethe (ed.), *Nobel Lectures, Chemistry 1996–2000* (World Scientific, Singapore, 2003)
50. A.G. MacDiarmid, edited by I. Grethe, *Nobel Lectures, Chemistry 1996–2000* (World Scientific, Singapore, 2003)
51. A.J. Heeger, edited by I. Grethe, *Nobel Lectures, Chemistry 1996–2000* (World Scientific, Singapore, 2003)
52. A.J. Heeger, S. Kivelson, J.R. Schrieffer, W.P. Su, *Rev. Mod. Phys.* **60**, 781 (1988) (and references therein)
53. S. Roth, H. Bleier, *Adv. Phys.* **36**, 385 (1987)
54. L. Yu (Ed.), *Solitons & Polarons in Conducting Polymers* (World Scientific, Singapore, 1988)
55. N. Greenham y R.H. Friend, edited by H. Ehrreich, F. Spaepen, *Solid State Physics*, Vol. 49, 1 (Academic Press, San Diego, 1995)
56. H.S. Nalwa (ed.), *Handbook of Nanostructured Materials and Nanotechnology*, Vol. 5: Organics, polymers, and biological materials (Academic Press, San Diego, 2000)
57. N. Tessler, Y. Preezant, N. Rappaport, Y. Roichman, *Adv. Mater.* **21**, 2741 (2009)
58. J.-L. Bredas, S.R. Marder (ed.), *The WSPC Reference on Organic Electronics: Organic Semiconductors*, vol. 1 Basic concepts, Vol. 2 Fundamental aspects of materials and applications (World Scientific, Singapore, 2015)
59. S. Kivelson, D.E. Heim, *Phys. Rev. B* **26**, 4278 (1982)
60. C.K. Chiang, C.R. Fincher Jr., Y.W. Park, A.J. Heeger, H. Shirakawa, E.J. Louis, S.C. Gau, A.G. MacDiarmid, *Phys. Rev. Lett.* **39**, 1098 (1977)
61. J. Tsukamoto, A. Takahashi, K. Kawasaki, *Japan J. Appl. Phys.* **29**, 125 (1990)

62. N.F. Mott, *Metal-Insulator Transitions*, 2nd. edn. (Taylor & Francis, London, 1990), p. 50
63. B.I. Shklovskii, A.L. Efros, *Electronic Properties of Doped Semiconductors* (Springer, Berlin, 1984), ch. 9
64. A.P. Chetverikov, W. Ebeling, M.G. Velarde, *Eur. Phys. J. B* **88**, 202 (2015)
65. M.G. Velarde, W. Ebeling, A.P. Chetverikov, *Int. J. Bifurcation Chaos* **15**, 245 (2005)
66. A.P. Chetverikov, W. Ebeling, M.G. Velarde, *Int. J. Bifurcation Chaos* **16**, 1613 (2006)
67. A. Ovchinnikov, *Soviet Phys. JETP* **30**, 147 (1970)
68. S. Barisic, *Phys. Rev. B* **5**, 932 (1972)
69. A.S. Dolgov, *Sov. Phys. Solid State* **28**, 907 (1986)
70. A. Sievers, S. Takeno, *Phys. Rev. Lett.* **61**, 970 (1988)
71. J.B. Page, *Phys. Rev. B* **41**, 7835 (1990)
72. S.A. Kiselev, S.R. Bickham, A.J. Sievers, *Phys. Rev. B* **48**, 13508 (1993)
73. G.P. Tsironis, *Chaos* **13**, 657 (2003)
74. D.K. Campbell, S. Flach, Yu.S. Kivshar, *Phys. Today* **57**, 43 (2004) (and references therein)
75. G. Iooss, G. James, *Chaos* **15**, 015113 (2005)
76. S. Aubry, *Physica D* **216**, 1 (2006)
77. S. Flach, A. Gorbach, *Phys. Rep.* **467**, 1 (2008) (and references therein)
78. A.A. Kistanov, S.V. Dmitriev, A.P. Chetverikov, M.G. Velarde, *Eur. Phys. J B* **87**, 211 (2014)
79. S. Dmitriev, A.P. Chetverikov, M.G. Velarde, *Physica Status Solidi (b)* **252**, 1682 (2015)
80. M.G. Velarde, A.P. Chetverikov, W. Ebeling, S.V. Dmitriev, V.D. Lakhno, *Procs. Estonian Acad. Sci.* **64**, 396 (2015)
81. J.C. Slater, *Quantum Theory of Molecules and Solids*, Vol. 4 (McGraw-Hill, New York, 1974)
82. J.P. Launay, M. Verdaguer, *Electrons in Molecules* (Oxford University Press, Oxford, 2014)
83. A.S. Davydov, *Solitons in Molecular Systems*, 2nd. edn (Reidel, Dordrecht, 1991)
84. P.L. Christiansen, A.C. Scott (eds.), *Davydov's Soliton Revisited. Self-trapping of Vibrational Energy in Protein* (Plenum Press, New York, 1990)
85. A.C. Scott, *Phys. Rep.* **217**, 1 (1992)
86. D. Hennig, A.P. Chetverikov, M.G. Velarde, W. Ebeling, *Phys. Rev. E* **76**, 046602 (2007)
87. M.G. Velarde, W. Ebeling, A.P. Chetverikov, *Int. J. Bifurcation Chaos* **18**, 3815 (2008)
88. O.G. Cantu-Ross, L. Cruzeiro, M.G. Velarde, W. Ebeling, *Eur. Phys. J. B* **80**, 545 (2011)
89. A.P. Chetverikov, W. Ebeling, M.G. Velarde, *Eur. Phys. J. B* **85**, 291 (2012)
90. A.P. Chetverikov, W. Ebeling, G. Röpke, M.G. Velarde, *Eur. Phys. J. B* **87**, 153 (2014)
91. M.G. Velarde, A.P. Chetverikov, W. Ebeling, E.G. Wilson, *Eur. Phys. Lett. EPL* **106**, 27004 (2014)
92. K.J. Donovan, E.G. Wilson, *Phil. Mag. B* **44**, 9 and 31 (1981)
93. K.J. Donovan, P.D. Freeman, E.G. Wilson, *J. Phys. C: Solid State Phys.* **18**, L275 (1985)
94. K.J. Donovan, E.G. Wilson, *J. Phys.: Condens. Matter* **2**, 1659 (1990)
95. K. Donovan, J.W.P. Elkins, E.G. Wilson, *J. Phys.: Condens. Matter* **3**, 2075 (1991)
96. E.G. Wilson, *J. Phys. C: Solid State Phys.* **16**, 6739 (1983)
97. A.M. Kosevich, A.S. Kovalev, *Soviet Phys. JETP* **40**, 891 (1975)
98. J.S. Zmuidzinas, *Phys. Rev. B* **17**, 3919 (1978)
99. A.V. Zolotaryuk, K.H. Spatschek, A.V. Savin, *Phys. Rev. B* **54**, 266 (1996)
100. M.G. Velarde, L. Brizhik, A.P. Chetverikov, L. Cruzeiro, W. Ebeling, G. Röpke, *Int. J. Quantum Chem.* **112**, 551 and 2591 (2012)
101. L. Brizhik, A.P. Chetverikov, W. Ebeling, G. Röpke, M.G. Velarde, *Phys. Rev. B* **85**, 245105 (2012)
102. R. Landauer, *IBM J. Res. Dev.* **5**, 183 (1961) [reprinted **44**, 261 (2000)]
103. J.A. Vaccaro, S.M. Barnett, *Proc. Roy. Soc. A* **467**, 1770 (2011)